



Cell adhesion and detachment on gold surfaces modified with a thiol-functionalized RGD peptide

Sang-Hee Yoon^{a,b,1}, Mohammad R.K. Mofrad^{a,*}

^a Molecular Cell Biomechanics Laboratory, Department of Bioengineering, University of California, Berkeley, CA 94720, USA

^b Department of Mechanical Engineering, University of California, Berkeley, CA 94720, USA

ARTICLE INFO

Article history:

Received 5 May 2011

Accepted 26 May 2011

Available online 3 August 2011

Keywords:

Cell adhesion

Cell detachment

Electrochemistry

Gold

Polyethylene glycol

Thiol-functionalized arginine-glycine-aspartic acid (RGD) peptide

ABSTRACT

The dynamic nature of cell adhesion and detachment is critically important to a variety of physiological and pathophysiological phenomena. Much, however, still remains uncertain and controversial about the mechanochemical players and processes involved in cellular adhesion and detachment. This leads to the need for quantitative characterization of the adhesion and detachment of anchorage-dependent cells. Here, cell adhesion and detachment up to subcellular level are examined using gold surfaces modified with a thiol-functionalized arginine-glycine-aspartic acid (RGD) peptide. A thiol self-assembled monolayer (SAM) on top of the gold surfaces is reductively desorbed with activation potential to spatiotemporally manipulate both cell adhesion and detachment. This method maintains cells of interest living and intact during experiments, making it possible to quantify cell adhesion and detachment as close as possible to *in vivo* conditions. Experimental characterizations for NIH 3T3 fibroblasts are carried out with a focus on the following issues: the effect of the size and geometric shape of gold surfaces on cell adhesion; the effect of cell confluency, cell shape, and activation potential magnitude on cell detachment; changes in the material properties of cells during cell detachment. The findings of this study should lead to better understanding of cellular dynamics in anchorage-dependent cells.

© 2011 Elsevier Ltd. All rights reserved.

1. Introduction

Cell adhesion and detachment processes are mediated by a complex biomolecules from both sides of the cell–matrix interface, fitting together like pieces of a three-dimensional puzzle. When cells adhere to extracellular matrix (ECM) components, integrins are activated; the activated integrins bind target ligands; the bound integrins cluster together by changing their conformation [1–3]. The cytoplasmic domain of the clustered integrins interacts with focal adhesion (FA) proteins (e.g., talin, focal adhesion kinase, vinculin, and paxillin) to form FAs, and then binds to actin filaments (Fig. 1, top) [4–6]. Likewise, the cell detachment or de-adhesion, essential to many cellular dynamic phenomena (e.g., cell migration), results from a concerted process involving this molecular machinery composed of a host of extracellular, transmembrane and cytoplasmic proteins.

Cell adhesion and detachment have profound effects on the behavior and function of anchorage-dependent cells. For example, cell adhesion and detachment are controlling parameters in a variety of biological phenomena (e.g., embryonic development, cancer metastasis, wound healing, etc.), and any abnormality in cell adhesion and detachment accompanies diverse pathophysiological consequences [1,3]. The quantitative characterization of the dynamics of cell adhesion and detachment is therefore essential for understanding a variety of pathophysiological phenomena.

Despite significant progress over the past decade in characterizing biomolecules and signaling pathways for cell adhesion and detachment, the *biophysical details* of cell adhesion and detachment still remain illusive [7,8]. Initially, the cell spreading and migration experiments were used to characterize cell adhesion and detachment. These multistep biological phenomena, however, provided their ambiguous and complicated roles in cell adhesion and detachment [9], and failed to quantify the dynamic nature of cell adhesion and detachment. Thus, a variety of other experimental methods which can manipulate cell adhesion or detachment has been developed. The techniques for cell adhesion manipulation were photolithography [10,11], e-beam lithography [12], dip-pen lithography [13], nanoimprint lithography [14], micro

* Corresponding author. Tel.: +1 510 643 8165; fax: +1 510 642 5835.

E-mail address: mofrad@berkeley.edu (M.R.K. Mofrad).

URL: <http://biomechanics.berkeley.edu/>

¹ Present address: Wyss Institute for Biologically Inspired Engineering, Harvard University, Cambridge, MA 02138, USA.

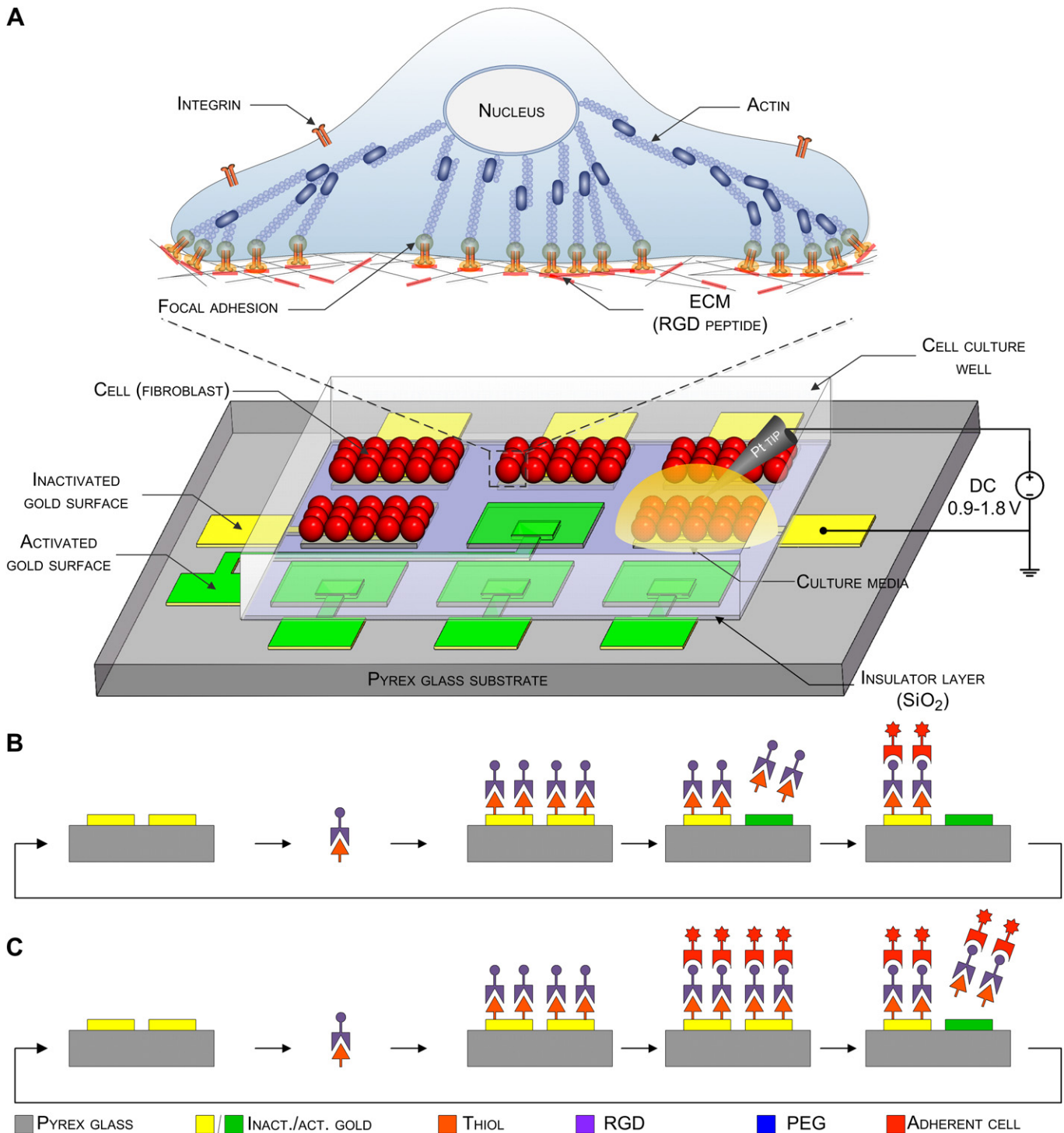


Fig. 1. An assay for spatiotemporally controlled manipulation of cell adhesion and detachment. (A) A schematic of the assay composed of identical gold surfaces, a SiO₂ insulator layer, and a Pyrex glass substrate. This assay is surface-modified with thiol-functionalized RGD peptide (for the gold surfaces) and PEG (for the Pyrex glass substrate) to spatiotemporally control cell adhesion and detachment. (B) Spatiotemporal manipulation of cell adhesion. Before cell adhesion manipulation, RGD peptide is bound to all gold surfaces via thiol and PEG is coated on the Pyrex glass substrate. On cell adhesion manipulation, the RGD peptide on a target gold surface (on the right side) is detached by activating the target gold surface with activation potential, followed by cell loading. The loaded cells adhere only to an inactivated gold surface (on the left side). (C) Spatiotemporal manipulation of cell detachment. Before cell detachment manipulation, cells are loaded and then adhere to all gold surfaces modified with a thiol-functionalized RGD. On cell detachment manipulation, the cells or one part of the cell is detached from a target gold surface (on the right side) with activation potential which yields the reductive desorption of a gold-thiol SAM. (For interpretation of the references to colour in this figure legend, the reader is referred to the web version of this article.)

contact printing [15,16], elastomeric stencil [17], ink-jet printing [18], optical tweezer [19], electrophoresis [20,21], and switchable surface [22]; the techniques for cell detachment manipulation were hydrodynamic shear force assay [23–29], centrifugal assay

[30–33], and micropipette aspiration [34–36]. These techniques successfully manipulated either cell adhesion or detachment. They were, however, designed not to characterize cell behavior during adhesion and detachment but to achieve cell adhesion or

detachment for next-step applications (e.g., cell patterning (or positioning), co-culture, etc.). Furthermore, these techniques featured unintended mechanical stimuli (cell denaturation [19], cell electrolysis [20,21], and cell rupture [23–36]) to cells of interest and considerably deformed the cells before experiments, thus resulting in inaccurate measurements [37]. Recently, electrochemical methods have been developed to characterize the cell adhesion and detachment of live and intact cells. Jiang et al. manipulate cell detachment using the electrochemical desorption of an EG₃-terminated SAM, showing the direction of polarization of attached mammalian cells determined their motility direction [38]. Inaba et al. [39] noninvasively harvested anchorage-dependent cells by means of the electrochemical desorption of a SAM of alkanethiol for tissue engineering applications. Guillaume-Gentil et al. [40] switched the biointerfacial properties of micro-patterned

domains through the spatiotemporally controlled dissolution and adsorption of polyelectrolyte coatings for co-culture of two different cells. Although these previous electrochemical methods controlled either cell adhesion or cell detachment, their success in characterizing cell adhesion or detachment was limited to qualitative results.

A new assay is proposed here to manipulate both cell adhesion and cell detachment at cellular and even subcellular levels, thus offering a platform to quantify the adhesion and detachment behavior of anchorage-dependent cells which are still living and intact during experiments. This assay has the following features in quantifying cell adhesion and detachment. First of all, the assay characterizes the cell adhesion and detachment behavior of living and intact cells. If the cells of interest are killed or receive any mechanical stimulus during experiments, the method will have

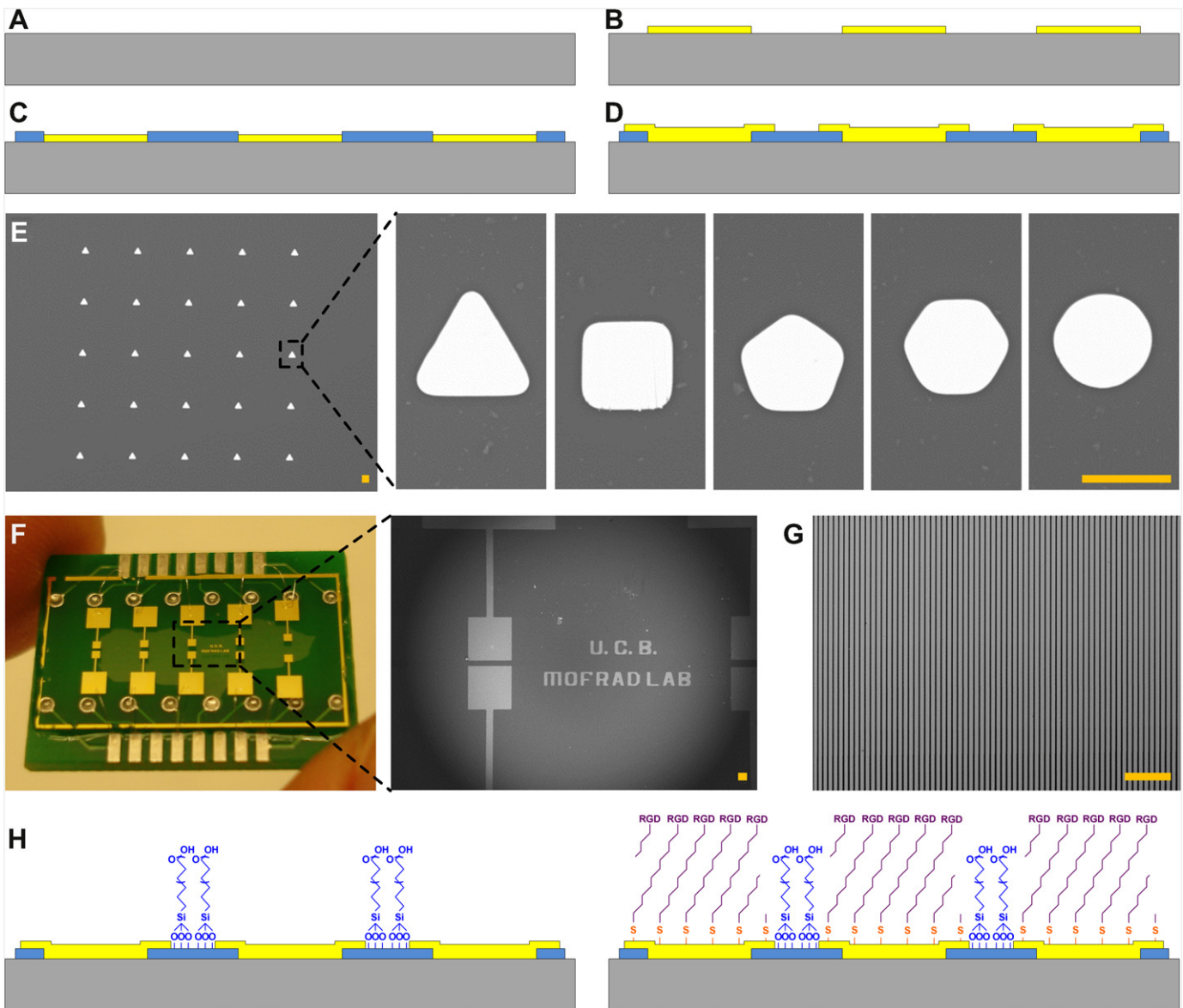


Fig. 2. Microfabrication and surface modification of the assay. (A–D) Microfabrication process: starting with a 4-inch Pyrex glass wafer (A); patterning a Cr/Au layer through photoresist patterning, Cr/Au layer deposition, and Cr/Au layer lift-off (B); patterning SiO₂ insulator layer through SiO₂ layer deposition, photoresist patterning, SiO₂ layer dry-etching, and photoresist removal (C); patterning the second Cr/Au layer using the same process used for the first Cr/Au layer (D). (E) Assay for cell adhesion manipulation, each gold surface of which is an equilateral triangle, square, regular pentagon, regular hexagon, or circle. (F) Assay for cell detachment manipulation. (G) Assay for subcellular detachment manipulation. (H) Surface modification process. The assay is incubated with a PEG solution to make its Pyrex glass substrate cell-resistant (left), and then incubated with a synthesized thiol-functionalized RGD solution to modify the gold surface cell-resistant (right). Scale bars of (E) and (G) are 10 μ m, and that of (F) is 100 μ m. (For interpretation of the references to colour in this figure legend, the reader is referred to the web version of this article.)

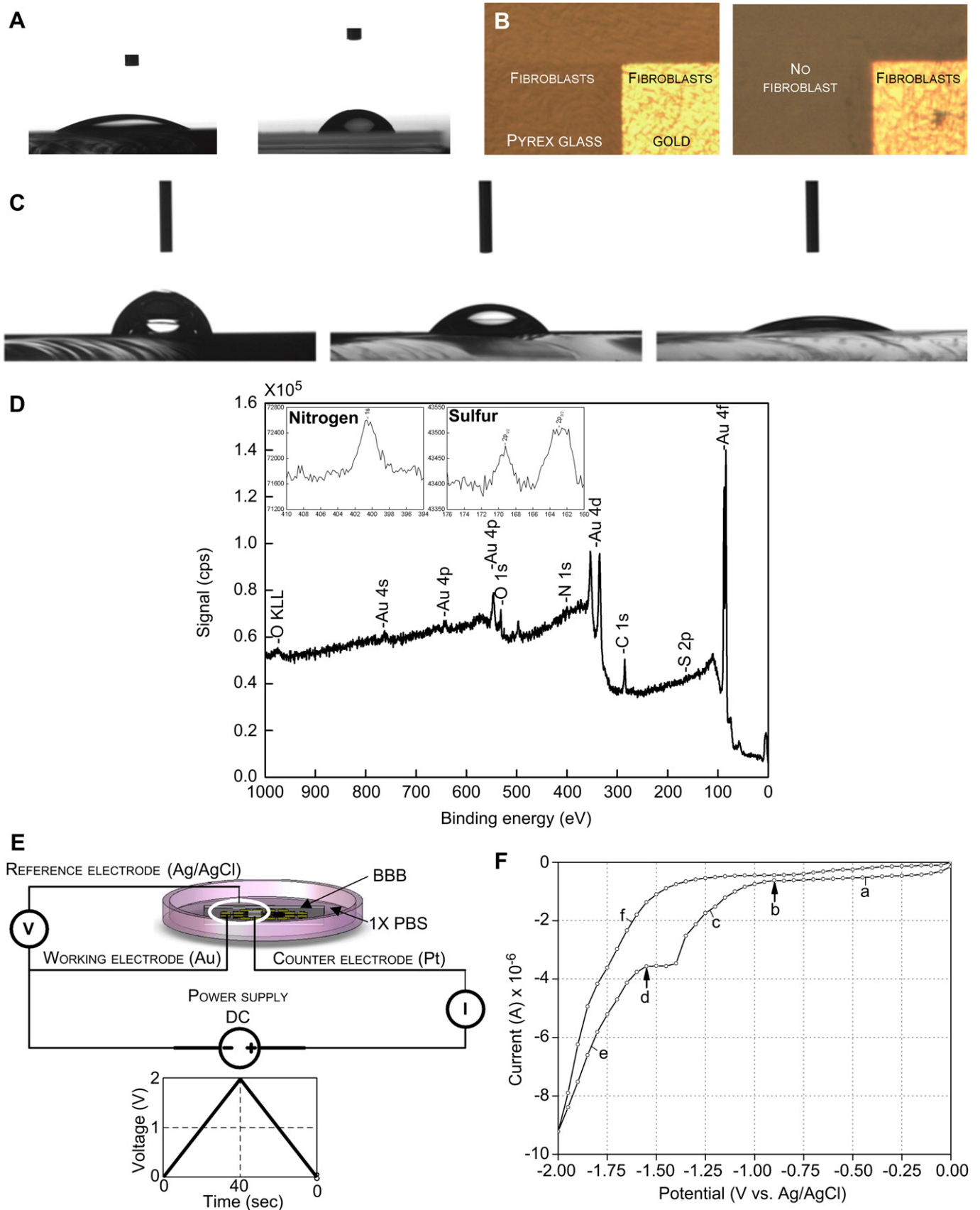


Fig. 3. Characterizations of the surface modifications of the assay and potentiodynamic electrochemical characterization of the reductive desorption of a gold-thiol SAM. (A) Contact angles measured from a Pyrex glass substrate before (left) and after (right) PEG modification. The contact angle is changed from $25.7 \pm 1.5^\circ$ to $61.5 \pm 3.8^\circ$ through PEG modification. (B) Cell (NIH 3T3 fibroblast) loading on a Pyrex glass substrate before (left) and after (right) PEG modification, showing the Pyrex glass substrate is changed from cell-adhesive to

a strong likelihood of disturbed results. Secondly, by employing an RGD peptide as a cell adhesion motif, this assay provides cells with a microenvironment that is as similar as possible to the real *in vivo* microenvironment. This is because a microenvironment is one of the most dominant factors in determining cell adhesion and detachment. Moreover, our assay can quantify both cell adhesion and cell detachment. These features make our method unique in characterizing cell adhesion and detachment on gold surfaces modified with a thiol-functionalized RGD peptide. In this paper, we characterize cell adhesion and detachment to address: dependence of cell adhesion on the size and geometric shape of gold surfaces; dependence of cell detachment on cell confluency, initial cell shape, and activation potential magnitude; changes in the material properties of cells detached at a subcellular level.

2. Materials and methods

2.1. Spatiotemporal manipulation of cell adhesion and detachment

The assay was composed of an array of identical gold surfaces, a SiO₂ insulator layer, and a Pyrex glass substrate (Fig. 1, bottom). The gold surfaces, patterned on the Pyrex glass substrate, provided sites for cell adhesion and detachment; the insulator layer between gold surfaces and Pyrex glass substrate was designed to prevent electrical short circuits during experiments as well as to minimize the distance between two neighboring gold surfaces. The Pyrex glass substrate and gold surfaces were modified with polyethylene glycol (PEG) and thiol-functionalized RGD peptide, respectively. The PEG modification on the Pyrex glass substrate was designed to achieve a cell-resistive surface where hydrated neutral PEG chains sterically repulsed cells; the thiol-functionalized RGD peptide modification was intended to make the gold surfaces cell-adhesive by tethering an RGD peptide to a gold surface via thiol compound. The thiol compound created a SAM on the gold surfaces following the spontaneous chemisorption,



where R is a substituent [41]. The thiol-functionalized RGD peptide therefore offered a cell (strictly speaking, integrin)-binding site which was almost same as *in vivo* microenvironment for cell adhesion and detachment.

The spatiotemporal manipulation of cell adhesion was implemented by selectively detaching the RGD peptide from the gold surfaces with activation potential of -0.9 to -1.8 V which yielded the reductive desorption of a gold-thiol SAM [42], following the electrochemical reaction



After surface modification with PEG and thiol-functionalized RGD peptide, the thiol-functionalized RGD peptide was detached by applying activation potential to a target gold surface, followed by sonification in a cell culture media and cell loading (Fig. 1B). The loaded cells adhered only to the inactivated gold surface on which a thiol-functionalized RGD peptide was placed because anchorage-dependent cells had substantially more affinity for cell adhesion to RGD peptide (on the inactivated gold surface) than to bare gold (on the activated gold surface).

The spatiotemporal manipulation of cell detachment using our assay was the same as that of cell adhesion except the order between gold surface activation and cell loading. When cells were loaded into the surface-modified assay, the loaded cells grafted to the RGD peptide. On cell detachment manipulation (Fig. 1C), the cells (or one part of the cell) were detached from the assay by applying activation potential which broke the chemical bonding between gold and thiol. When the detached cells sensed no mechanical anchorage (focal adhesion) to the gold surfaces, they started to retract by liquefying their cytoskeleton and changing the length of actin filaments.

2.2. Assay microfabrication

The assay was fabricated on a 4-inch Pyrex glass wafer with a thickness of 500 μm (Fig. 2A). After cleaning it with a piranha solution of 1:1 v:v 96% sulfuric acid (H₂SO₄) and 30% hydrogen peroxide (H₂O₂) for 10 min, 1 μm -thick LOR resist (LOR 10A, MicroChem Corp.) was spin-coated at 4000 rpm for 40 s, followed by soft

baking at 170 °C for 5 min. A 2 μm -thick positive photoresist (S1818, Rohm and Haas Corp.) was spin-coated on the LOR resist at 4000 rpm for 40 s for double-layer resist stacking, followed by soft baking at 110 °C for 1 min. An optical lithography was made to pattern the double-layer resist before e-beam evaporation process. The next was a deposition of 5 nm-thick chromium (Cr) adhesion layer and 100 nm-thick gold (Au) layer on the wafer. The Cr/Au-deposited wafer was immersed in an organic solvent mixture (BAKER PRS-3000 Stripper, Mallinckrodt Baker, Inc.) at 80 °C for 4 h to lift off the double-layer resist (Fig. 2B). Next, a 2500 Å-thick SiO₂ insulator layer was deposited by plasma-enhanced chemical vapor deposition (PECVD) process. This insulator layer was dry-etched to pattern through-holes for electrical interconnection between first and second Cr/Au layers (Fig. 2C). Finally, the second Cr/Au layer was deposited and patterned by using the same method for the first one (Fig. 2D). We fabricated three kinds of assays: assay for cell adhesion manipulation (Fig. 2E) where each gold surface has the same geometric shape (e.g., equilateral triangle, square, regular pentagon, regular hexagon, or circle) and the same size (e.g., 9 μm^2 , 25 μm^2 , 64 μm^2 , 100 μm^2 , 225 μm^2 , 400 μm^2 , 625 μm^2 , or 900 μm^2); assay for cell detachment manipulation (Fig. 2F) where each gold surface is 500 μm in length and 500 μm in width; assay for subcellular detachment manipulation where each gold line is 10 μm in width and 3 μm in distance between two neighboring gold lines (Fig. 2G). The microfabricated assay was wire-bonded in a chip carrier (Fig. 2F).

2.3. PEG modification on Pyrex glass substrate

Before PEG modification, the microfabricated assay was cleaned with an oxygen plasma chamber (PM-100 Plasma Treatment System, March Plasma Systems, Inc.) at 100 W for 30 s. The assay was then incubated with 2% v/v m-PEG silane (CI-PEG silane, Gelest) and 1% v/v hydrochloric acid (HCl, Fisher Scientific) dissolved in anhydrous toluene (Fisher Scientific) for 2 h (Fig. 2H, left). This process was carried out in a glove box under a nitrogen purge to avoid atmospheric moisture. The incubated assay was rinsed in fresh toluene and ethanol, dried with nitrogen, and cured at 120 °C for 2 h. The surface-modified assay was stored in a vacuum desiccator until the next surface modification.

2.4. Thiol-functionalized RGD peptide modification on gold surface

The gold surfaces of the assay were modified with a thiol-functionalized RGD peptide whose solution was synthesized by chemically combining cyclo (Arg-Gly-Asp-D-Phe-Lys) (c(RGDfK), C₂₇H₄₁N₉O₇, Peptides International, Inc.) with dithiobis(succinimidylundecanoate) (C₃₀H₄₈N₂O₈S₂, Dojindo Molecular Technologies, Inc.) as follows. The c(RGDfK) was dissolved in dimethylsulfoxide (DMSO, Sigma-Aldrich) to get 1 mM aliquot and stored at -20 °C. This reaction was made in a glove box under a nitrogen purge to protect the c(RGDfK) from exposure to atmospheric moisture. The maximum storage period of this solution was limited to 15 days because this peptide easily lost its characteristics (e.g., anchor for $\alpha_v\beta_3$ integrin). The dithiobis(succinimidylundecanoate) was also stored in 1 mM aliquot in DMSO at -20 °C. This preparation was also done in moisture-free environment. Before gold surface modification, both aliquots were warmed to room temperature in a desiccator. The c(RGDfK) aliquot was mixed with 1% v/v triethylamine (Fisher Scientific) for 5 min to make all primary amines of a lysine amino acid unprotonated. The same volume of the dithiobis(succinimidylundecanoate) was added to the c(RGDfK) aliquot, and then mixed well using a vortex mixer for 4 h to synthesize thiol-functionalized RGD peptide solution. For the gold surface modification (Fig. 2H, right), the PEG-modified assay was incubated with this solution for 1 h at room temperature to promote a spontaneous chemisorption between thiol and gold, followed by sonification in DMSO for 3 min, rinse in ethanol and phosphate buffered saline (PBS, Sigma-Aldrich) to eliminate an unbound thiol-functionalized RGD peptide from gold surfaces. The thiol made a SAM on the gold surfaces, thereby tethering an RGD peptide to the gold surfaces.

2.5. Contact angle measurement

The contact angles of PEG-modified Pyrex glass substrate and thiol-functionalized RGD peptide-modified gold surface were measured with a contact angle measurement system, goniometer (KRÜSS582, KRÜSS). A sessile drop mode was used to estimate the wetting properties of the above two surfaces. The contact angles were averaged from 10 measurements. The contact angle of PEG-modified Pyrex glass substrate was compared to that of pure Pyrex glass substrate, and the contact angle of thiol-functionalized RGD peptide-modified gold surface was compared to those of bare gold surface and thiol-modified gold surface.

cell-resistive. (C) Contact angles measured from bare gold ($67.3 \pm 2.5^\circ$, left), thiol-modified gold ($53.3 \pm 1.3^\circ$, center), and thiol-functionalized RGD peptide-modified gold ($24.6 \pm 2.8^\circ$, right). (D) XPS survey spectrum of the gold surface modified with a thiol-functionalized RGD peptide. Detected are a gold peak from a gold surface, a sulfur peak from thiol, a nitrogen peak from the amine group of an RGD peptide, and carbon and oxygen peaks from the carboxylic acid group of an RGD peptide. (E) Experimental setup for potentiodynamic electrochemical characterization where the gold surface of the assay, a platinum electrode, and an Ag/AgCl electrode work as working, counter, and reference electrodes, respectively. (F) Cyclic voltammetry measured from the gold surface modified with a thiol-functionalized RGD peptide, indicating the reductive desorption of the gold-thiol SAM starts and finishes at -0.9 V and -1.55 V respectively and gets maximized at -1.4 V. (For interpretation of the references to colour in this figure legend, the reader is referred to the web version of this article).

2.6. X-ray photoelectron spectroscopy (XPS) sample preparation and characterization

An XPS survey scan was used to confirm the existence of an RGD peptide linked to gold surfaces via thiol after thiol-functionalized RGD peptide modification. An XPS sample was prepared on a 4-inch silicon wafer e-beam evaporated with 5 nm Cr adhesion layer and 50 nm Au layer. This wafer was immersed for 2 h in the prepared thiol-functionalized RGD peptide solution. A bare gold sample without any surface modification was run as a control experiment. The XPS analysis was carried out with a customized ESCA (Omicron Nano Technology) at 1×10^{-8} Torr, and all measured spectra were referenced to the position of the Au 4f peaks. The scans were collected over a range of 20 eV around the peaks of interest with a pass energy of 23.5 eV.

2.7. Potentiodynamic electrochemical characterization of reductive desorption of gold-thiol SAM

A silicon wafer e-beam evaporated with 5 nm-thick Cr and 50 nm-thick Au was modified with a thiol-functionalized RGD peptide to prepare a cyclic voltammetry sample. This thiol-functionalized RGD peptide-modified gold surface was used as a working electrode while a platinum electrode and an Ag/AgCl electrode were used as counter electrode and reference electrode, respectively (see Fig. 3E). A voltage supplied by a DC power source (B&K Precision Corporation) was applied between the gold-thiol SAM (or Ag/AgCl electrode) and the platinum electrode. The cyclic voltammetry was carried out in the Dulbecco's phosphate buffered saline (DPBS (pH 7.4), Sigma–Aldrich) solution with an EG&G potentiostat model 362 (AMETEK Princeton Applied Research). A scan started cathodically from 0 V to -2 V, then anodically back to 0 V at a scan rate of 50 mV s^{-1} .

2.8. Cell culture

The NIH 3T3 mouse embryonic fibroblast cell (NIH 3T3 fibroblast) was cultured in Dulbecco's modified eagle medium (DMEM, GIBCO™) supplemented with 10% fetal bovine serum (FBS, GIBCO™) and 1% Penicillin–Streptomycin (GIBCO™) at 37°C in a humidified atmosphere of 5% CO_2 . The cell was passaged every 4 day as follows. The cell was washed 1 time in $1 \times$ PBS and trypsinized with 0.5% Trypsin–EDTA solution (Sigma–Aldrich). After centrifuging the cell, it was inoculated into a new Petri dish. The NIH 3T3 fibroblast with a passage number of 5–20 was used in the experimental studies. Before each experiment, the surface-modified assay was sterilized with 70% ethanol, washed twice with $1 \times$ PBS, and placed in a Petri dish containing 5 ml cell culture medium with a cell suspension of about 1×10^6 cells/ml. For subcellular detachment experiments, the cell suspension concentration was changed into 1×10^4 cells/ml. After 1 h, unadhered NIH 3T3 fibroblast was removed by additional wash in PBS, followed by culture medium replacement. All experiments were carried out after 24 h of cell loading in a self-designed chamber with a humidified atmosphere of 5% CO_2 and at 37°C .

2.9. Immunofluorescence microscopy

Cells were fixed with 4% formaldehyde solution (Fisher Scientific) in chilled PBS for 15 min. The fixed cells were permeabilized with $200 \mu\text{l}$ 0.5% Triton X-100 (Sigma–Aldrich) in PBS at room temperature for 10 min and were washed 3 times with PBS, followed by blocking non-specific binding using 3% non-fat dry milk in PBS at 4°C for 1 h and washing the cells once with PBS. $10 \mu\text{l}$ methanolic stock solution of rhodaminephalloidin (Biotium, Inc.) was diluted with $200 \mu\text{l}$ PBS with 1% Bovine Serum Albumin (BSA, Fisher Scientific) for each assay. The assay was incubated with this solution for 20 min at room temperature and washed 2 or 3 times with PBS. For nucleus staining, ProLong® gold antifade reagent with DAPI (Invitrogen) was added into the cells. Immunofluorescent images were obtained on an inverted fluorescent microscope (Axiovert 200, Carl Zeiss MicroImaging, Inc.).

2.10. Atomic force microscopy (AFM) indentation

The elastic modulus of the detached cytoskeleton of cells was measured with an Autoprobe CP atomic force microscope system (Park Science Instruments). All measurements were made at a low-indentation-speed of 10 nm/s to suppress a viscous damping effect in quantifying the elastic modulus of cells. The elastic modulus was determined by measuring the deflection of an AFM tip (HYDRA2R–100N, Nanoscience Instruments, Inc.) which indents the detached cell. The AFM tip with a nominal spring constant of 0.011 N/m was calibrated so that its real spring constant was determined as $0.016 \pm 0.005 \text{ N/m}$, which was used in the AFM indentation.

3. Results and discussion

3.1. Surface modifications

Two kinds of surface modifications, made on the assay, were examined by contact angle measurement and XPS survey. The contact angle measured from a PEG-modified Pyrex glass substrate was $61.5 \pm 3.8^\circ$ (mean \pm standard deviation, averaged from 10 measurements), whereas that measured from an untreated Pyrex glass substrate was $25.7 \pm 1.5^\circ$ (Fig. 3A). This shows the PEG-modified Pyrex glass substrate is changed to have strong hydrophobicity through PEG modification and consequently prevents cell adhesion (and protein fouling). The effect of PEG modification on cell adhesion was also investigated with cell loading tests using NIH 3T3 fibroblasts (Fig. 3B). The images obtained after 24 h of cell loading show the Pyrex glass substrate is modified into cell-resistive as intended. A thiol-functionalized RGD peptide modification on gold surfaces was characterized using the same method. The contact angles measured from bare gold, thiol-modified gold, and thiol-functionalized RGD peptide-modified gold were $67.3 \pm 2.5^\circ$, $53.3 \pm 1.3^\circ$, and $24.6 \pm 2.8^\circ$, respectively (Fig. 3C). This modification was also characterized by an XPS survey scan. The XPS survey spectrum measured from an RGD/thiol/Au interface (Fig. 3D) shows the following results: the peaks of Au 4s, Au 4p, Au 4d, and Au 4f indicate the presence of e-beam evaporated gold (Au(111)); the peaks of S $2p_{1/2}$ and S $2p_{3/2}$ (right inset) mean sulfur from thiol compound is in existence on the RGD/thiol/Au interface; the peaks of C 1s, O 1s, O KLL, and N 1s (left inset) demonstrate there are carbon, oxygen, and nitrogen from the amine functional group ($-\text{NH}_2$) and carboxylic acid functional group ($-\text{COOH}$) of an RGD peptide. For reference, hydrogen was not detected due to XPS working principle. This XPS survey spectrum demonstrates the thiol-functionalized RGD peptide modification on gold surfaces is well made as designed and provides a cell-binding site as close as possible to *in vivo* microenvironment.

3.2. Reductive desorption of gold-thiol SAM

The rapid desorption of a gold-thiol SAM with negative potential was investigated by measuring a cyclic voltammetry in DPBS solution (pH 7.4) using a three-electrode system where the gold surface (of the assay), a platinum electrode, and an Ag/AgCl electrode worked as working, counter, and reference electrodes, respectively (Fig. 3E). The cyclic voltammetry was measured from the working electrode as a function of the applied potential with respect to the counter electrode (Fig. 3F). At a section “a” (0 V to -0.9 V), the current was negligible. This means the gold-thiol SAM impedes electron transfer across an electrolyte–electrode interface due to no reductive desorption of the SAM. The reductive desorption of the SAM started and finished at point “b” (-0.9 V) and point “d” (-1.55 V), respectively. This electrochemical reaction was maximized at -1.4 V. This measurement indicates the optimum potential to complete this electrochemical reaction is -0.9 V to -1.55 V, around -1.4 V. The release of an RGD peptide from a gold surface by applying negative potential to a gold-thiol SAM is also verified.

3.3. Cell adhesion of anchorage-dependent cells

The cell adhesion of anchorage-dependent cells was characterized using our method. NIH 3T3 fibroblasts were detached from gold surfaces modified with a thiol-functionalized RGD peptide. To demonstrate the spatiotemporal manipulation of cell adhesion on the gold surfaces, we used an assay composed of two-by-one gold surfaces where the gold surface on the left side was activated with activation potential of -1.5 V but that on the right side was

inactivated. When cells were loaded, the loaded cells adhered only to the gold surface on the right side, as shown in optical and immunofluorescent images (Fig. 4A). This shows anchorage-dependent cells make integrin-mediated cell adhesion which has much higher affinity for RGD peptide than for bare gold. The dependence of cell adhesion at a single cell level on the size and geometric shape of a gold surface was also studied with forty types of the assay. Each array was designed to have twenty five identical gold surfaces whose size was $9 \mu\text{m}^2$, $25 \mu\text{m}^2$, $64 \mu\text{m}^2$, $100 \mu\text{m}^2$, $225 \mu\text{m}^2$, $400 \mu\text{m}^2$, $625 \mu\text{m}^2$, or $900 \mu\text{m}^2$ and shape was a n -sided regular polygon ($n = 3, 4, 5, 6, \infty$ (circle), Fig. 4B). NIH 3T3 fibroblasts were loaded into the surface-modified assays at a cell suspension concentration of 1×10^6 cells/ml. As an index for quantifying cell adhesion at a single cell level, a cell adhesion ratio (CA-ratio), defined as the ratio of the number of gold surfaces with cell adhesion to the total number of gold surfaces, was measured as a function of the size and geometric shape of a gold surface (Fig. 4C). The measured CA-ratio provides the following biological facts. First, the CA-ratio in a single cell level is proportional to the size of a gold surface, and the minimum size of a gold surface for single cell adhesion is the diameter of a cell in a floating state ($10 \mu\text{m}$ for NIH 3T3 fibroblast). This indicates an anchorage-dependent cell can make its FAs through cell-to-substrate interaction when it has a cell-binding site which is larger than (or at least comparable to) the size of a single cell. Secondly, a cell wants to make its adhesion on the circumferential zone of a gold surface rather than the central zone. The CA-ratio is therefore proportional to the circumferential length of a gold surface when each gold

surface has the same area. This is likely because the circumferential zone has its microbump due to the side faces of the deposited Cr/Au layer so that provides additional cell-binding sites. The micro-size pattern is known to enhance cell adhesion [42]. These findings let us know how to design a gold surface for single cell adhesion. The size of a gold surface should be larger than the size of a single cell in a floated condition. The geometric shape of a gold surface, when its area is limited, needs to be an equilateral triangle or square. This is because the circumferential length, S , of an n -sided regular polygon with a side length of l and a surface area of A is inversely proportional to the number of sides, n , of the regular polygon, $S = nl = 2\sqrt{nA} \tan(\pi/n)$ (Fig. 4C, inset).

3.4. Cell detachment of anchorage-dependent cells at a cellular level

The cell detachment of anchorage-dependent cells was explored at a cellular level. An entire cell (NIH 3T3 fibroblast) was detached from gold surfaces modified with a thiol-functionalized RGD peptide, thus characterizing the effect of cell confluency, initial cell shape (projected area), and activation potential magnitude on cell detachment behavior. The cell detachment experiments were performed for five cell confluency conditions of 0% (single or two cells, Fig. 5A), 25% (Fig. 5B), 50%, 75%, and 100% (fully confluent cells, Fig. 5C). A cell detachment or de-adhesion time (CD-time), τ , defined as the time required for detaching 95% of cells from a gold surface, was measured as an index for evaluating cell detachment. The CD-times measured from five cell confluency conditions with activation potential of -1.5 V were $45.2 \pm 6.8 \text{ s}$, $36.7 \pm 8.7 \text{ s}$,

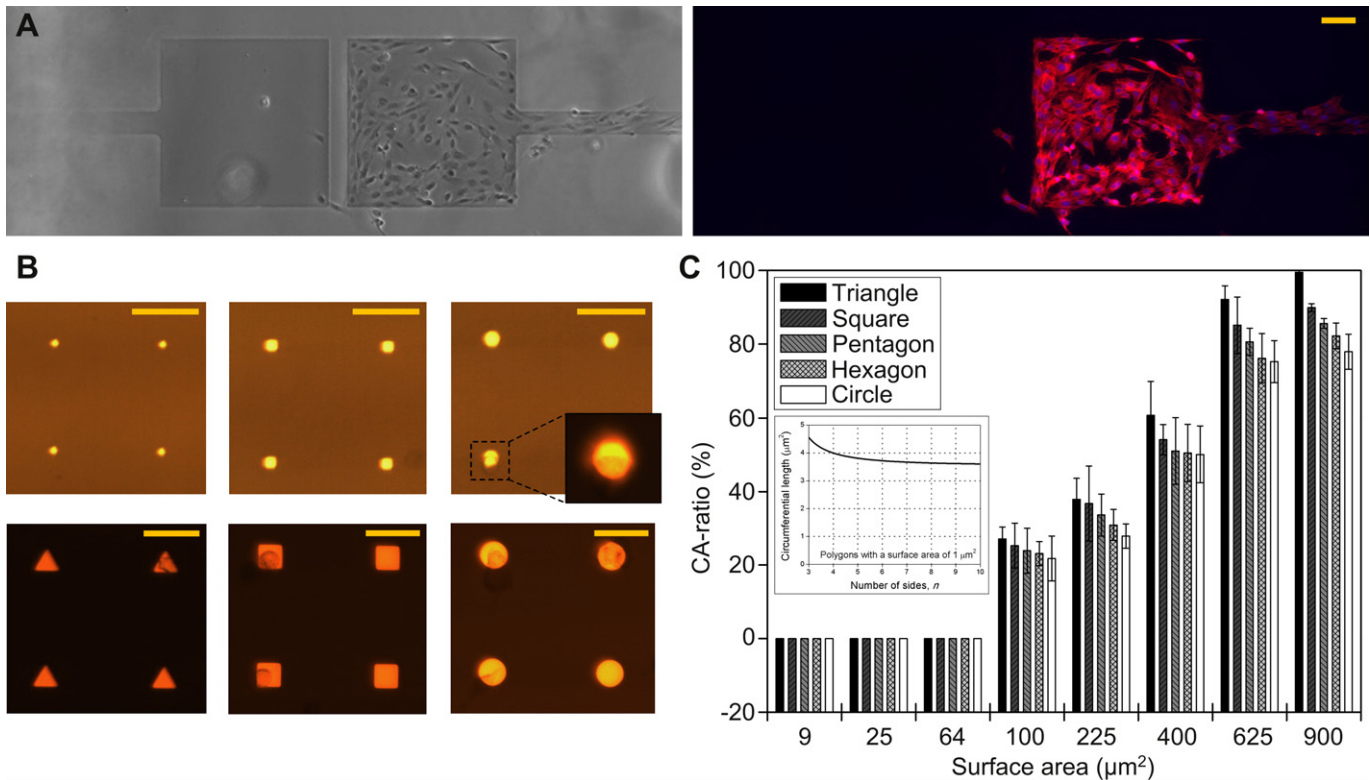


Fig. 4. Characterization of the cell adhesion of anchorage-dependent cells on gold surfaces modified with a thiol-functionalized RGD peptide. (A) Optical and immunofluorescent images of the spatiotemporal manipulation of cell adhesion. A two-by-one assay where a left gold surface is activated but a right one is inactivated is used here. Cells are stained for actin with rhodaminephalloidin (red) and for cell nucleus with DAPI (blue). (B) Single cell adhesion to a variety of gold surfaces with different size and shape. No cell adhesion is made on $25 \mu\text{m}^2$ -sized equilateral triangle gold surfaces (first from left) and $64 \mu\text{m}^2$ -sized square gold surfaces (second) with a cell suspension concentration of 1×10^6 cells/ml. Cell adhesions are made on 25% of $100 \mu\text{m}^2$ -sized regular hexagonal gold surfaces (third), 25% of $225 \mu\text{m}^2$ -sized equilateral triangle gold surfaces (fourth), 50% of $400 \mu\text{m}^2$ -sized square gold surfaces (fifth), and 75% of $625 \mu\text{m}^2$ -sized circle gold surfaces (sixth). (C) CA-ratio as a function of the size and geometric shape of gold surfaces. Inset shows the circumferential length of polygons as a function of number of sides when the polygons have the same surface area. Scale bar of (A) is $100 \mu\text{m}$, and those of (B) are $50 \mu\text{m}$. (For interpretation of the references to colour in this figure legend, the reader is referred to the web version of this article).

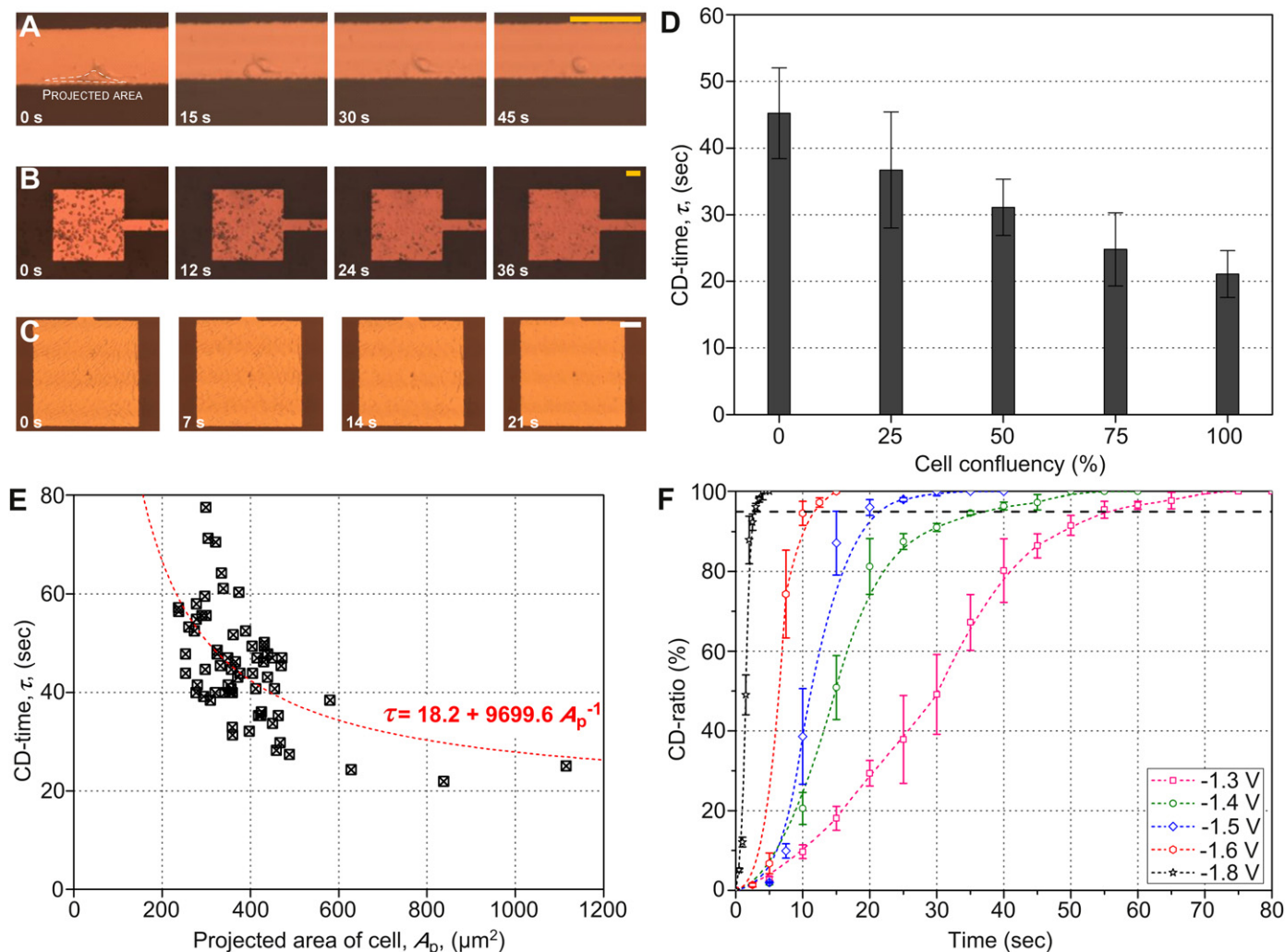


Fig. 5. Characterization of cell detachment at a cellular level. (A) Optical sequential images showing the spatiotemporal manipulation of the cell detachment of two cells (0% cell confluency) when activation potential is -1.2 V. The measured CD-time is 45.2 ± 6.8 s. (B) Cell detachment of 25% confluent cells whose average CD-time is 36.7 ± 8.7 s. (C) Cell detachment of 100% confluent cells whose average CD-time is 21.1 ± 3.5 s. (D) CD-time as a function of cell confluency with a negative potential of -1.5 V where 0% cell confluency means single or two cells. The measured CD-time is inversely proportional to cell confluency. (E) CD-time, τ (sec), as a function of the projected area of a cell, A_p (μm^2), measured from single cells with activation potential of -1.5 V. The measured CD-time is inversely proportional to the projected area of a cell, $\tau = 18.2 + 9699.9/A_p$. (F) CD-ratio as a function of activation time and potential measured from 100% confluent cells.

31.1 ± 4.2 s, 24.8 ± 5.5 s, and 21.1 ± 3.5 s, respectively (Fig. 5D). All data were averaged from at least 10 measurements. The measured CD-time was inversely proportional to cell confluency. This indicates cell-to-cell interaction through which cells are connected to each other at a fully confluent condition has a correlation to cell detachment. To detach a cell from a substrate, we need to break its cell-to-substrate interaction as well as cell-to-cell interaction to neighboring cells. The detachment of one cell therefore allows neighboring cells to be detached fast by providing a vertical force through cell-to-cell interaction. The relation between CD-time and initial cell shape (projected area), A_p , was also explored at a single cell condition (Fig. 5E). The projected area of a cell was calculated from the optical images of adhered single cells before cell detachment. The images were analyzed using an image processing program, ImageJ (National Institutes of Health, USA). The measured CD-time had an inverse relation to the projected area of a cell, represented as $\tau(\text{sec}) = 18.2 + 9699.9/A_p(\mu\text{m}^2)$. The projected area of a cell means the degree of tension stress within the cell, cytoskeletal stress. That is, a cell with a large projected area has higher cytoskeletal stress than a cell with a narrow projected area. Thus, the cell with a relatively large projected area is detached fast

due to its high cytoskeletal stress, indicating in-plane cytoskeletal stress is also closely related to out-of-plane cell behavior, cell detachment. The dependence of cell detachment on activation potential magnitude was also examined. A CD-ratio was measured by counting the ratio of the number of detached cells to the number of all cells as activation potential was changed from -1.3 V to -1.8 V (Fig. 5E). The CD-ratio was on the decrease as the activation potential was on the increase. This is because the reductive desorption of gold-thiol SAM gets faster as activation potential increase (Fig. 3F). The measured CD-ratio was monotonically increasing with two inflection points, s-shape curve. This clearly demonstrates there is a large deviation in the integrin binding to ECM and other cells which is related to cell-to-substrate and cell-to-cell interactions, respectively.

3.5. Cell detachment of anchorage-dependent cells at a subcellular level

The subcellular detachment behavior of anchorage-dependent cells was also explored by our assay which releases one part of a cell from the gold lines. The assay composed of gold lines with

a width of 10 μm and a gap of 3 μm (Fig. 2G) was used for this characterization. When one part of a NIH 3T3 fibroblast was detached with a single activation of -1.5 V , the retracted its detached cytoskeleton within 16 s (Fig. 6A). This fast retraction, compared to cell detachment at a cellular level, is because the single cell has a higher strain (or stress) than cells in a confluent condition. The single cell which has no constraint or interaction provided by other cells stretches itself as wide as possible so that it is always under relatively high strain (or stress). In the next subcellular detachment, one part of the single cell was sequentially detached with a series of activations where the first activation (activation 1) was followed by the second one (activation 2) after 16 s of the first activation (Fig. 6B). This subcellular detachment with sequential activations reveals: repetitive activations to a cell within dozens of seconds do not damage the cell's viability; the amount of subcellular detachment is adjustable by the sequential activation of gold surfaces which are located below the cell of interest; cell motility would be guided by spatiotemporal subcellular detachments on a large-scale assay.

3.6. Changes in viscoelastic properties during subcellular detachment

The changes in the viscoelastic properties of a NIH 3T3 fibroblast during its subcellular detachment were also quantified by detaching one part of the cell using this platform. First of all, the detached cell was assumed as isotropic and viscoelastic. The retraction motion of the detached cytoskeleton of a cell was described with a standard linear viscoelastic solid model composed of two springs, k_1 and k_2 , and one dashpot, c (Fig. 6C, top). From this model, a normalized-strain, ε^* , at retraction step (STEP II, Fig. 6C (bottom)) was mathematically expressed as [43]

$$\varepsilon^* = \frac{\varepsilon(t - t_2)}{\varepsilon_0} = \left(1 - \frac{k_2}{k_1 + k_2}\right) e^{-\frac{k_2}{c}(t - t_2)}, \quad (3)$$

where ε_0 is the initial strain of the cell at its protrusion step (STEP I, $0 < t \leq t_1$). The changes in the viscoelastic properties of the detached (and then retracting) cytoskeleton were measured by combining (3) with

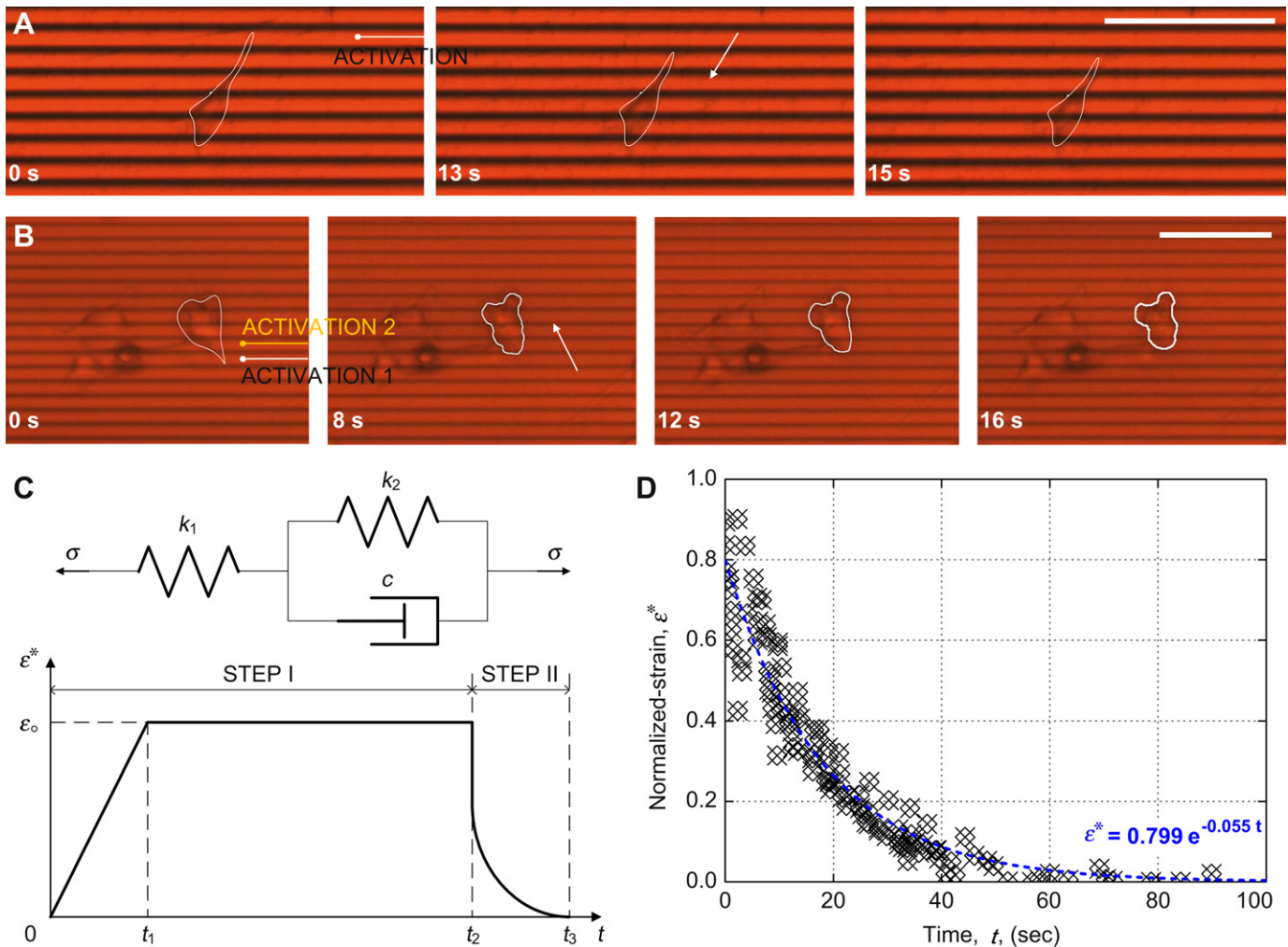


Fig. 6. Subcellular detachment manipulation using the gold lines modified with a thiol-functionalized RGD peptide and its applications to cellular dynamics characterizations. (A) Subcellular detachment using a single activation. One part of a cell is detached, and in turn the detached cytoskeleton starts to retract. (B) Subcellular detachment using a series of activations. One part of the cell is sequentially detached from the gold lines. (C) Continuum model to describe the retraction of a detached cytoskeleton where the cell is assumed as a homogeneous standard linear viscoelastic solid (top). Strain profile of an anchorage-dependent cell during cell adhesion and detachment (bottom). When a cell adheres to a substrate ($t = 0$), the cell extends its protrusion and adheres again ($0 < t \leq t_1$); the nucleus of the cell translocates ($t_1 < t \leq t_2$); one part of the cell is detached and retracts ($t_2 < t \leq t_3$). (D) Normalized-strain as a function of time obtained from single cells which are detached at a subcellular level. Arrows of (A) and (B) indicate the retraction direction of detached cytoskeleton. Scale bars of (A) and (B) are 100 μm . (For interpretation of the references to colour in this figure legend, the reader is referred to the web version of this article).

two experimental results: time-sequential images of the retraction motion of the detached cytoskeleton (obtained from twenty cells detached at a subcellular level) and AFM indentation results on the detached cytoskeleton. From the time-sequential images of subcellular detachment, the normalized-strain of the detached cytoskeleton was described as $\varepsilon^* = 0.799e^{-0.055t}$ (Fig. 6D). Based on the AFM indentation results on 10 samples [43], the total elastic modulus of the detached cytoskeleton ($k_{\text{total}} = k_1 k_2 / (k_1 + k_2)$) was determined as 1320 ± 310 Pa. These experimental results with (3) determined the viscoelastic properties of the detached cytoskeleton ($k_1 = 6567$ Pa, $k_2 = 1652$ Pa, and $c = 30037$ Pa s). Compared to the previous results ($k_{\text{total}} > 4000$ Pa and $c < 100$ Pa s) obtained from the adhered (not detached) cytoskeleton of fibroblasts [44,45], the detached cytoskeleton showed a three-times decrease in its elastic modulus and a thirty-times increase in its damping coefficient. This measurement suggests that a detached cytoskeleton becomes softer, and consequently has a remarkable increase in its damping coefficient after a few seconds of subcellular detachment. This phenomenon is likely owing to the gel–sol transition of actin filaments at cell detachment which changes the viscoelastic properties of the detached cytoskeleton. The subcellular detachment depolymerizes the cross-linked network of actin filaments. Thus, the structural strength of the detached cytoskeleton decreases, but its viscous damping capacity increases. This result shows that the subcellular adhesion/detachment platform can be further exploited for studies of cellular rheology and for quantification of viscoelastic properties of the cytoskeleton to supplement computational modeling efforts [46,47].

4. Conclusion

We have developed a method for the spatiotemporal manipulation of cell adhesion and detachment at cellular and even subcellular levels, thus quantitatively characterizing the adhesion and detachment behaviors of anchorage-dependent cells on gold surfaces modified with a thiol-functionalized RGD peptide. Our assay composed of an array of identical gold surfaces patterned on a Pyrex glass substrate is surface-modified with a thiol-functionalized RGD peptide. This assay manipulate cell adhesion and detachment using the reductive desorption of a gold-thiol SAM with activation potential of -0.9 V to -1.8 V, while maintaining cells of interest living and intact. In the experiments using NIH 3T3 fibroblasts, cell adhesion is proportional to the size of the gold surface, and is made on the circumferential zone of the gold surface rather than the central zone. These findings lead to several propositions for gold surface design: the gold surface for single cell adhesion must be larger than (or at least comparable to) the size of a single cell in a floating state; the geometric shape of the gold surface, when its area is limited, needs to be an equilateral triangle or square. Cell detachment behavior at a cellular level, characterized here, yields the following results: cell-to-cell interaction is one of the main factors which determine the velocity of cell detachment; a fully stretched cell with a relatively large projected area is detached fast, indicating the in-plane stress within a cell has a correlation with an out-of-plane cell behavior (cell detachment). In the characterization on subcellular detachment, the detached (and then retracting) cytoskeleton experiences a three-times decrease in its elastic modulus and also a thirty-times increase in its damping coefficient within a few seconds, showing cell detachment has a dynamic nature. Extrapolation of this method to other anchorage-dependent cells might help us to investigate critical cellular function and behavior, thereby leading to a better understanding of cellular dynamics. Ongoing work is focusing on more in-depth control of cell motility by developing a large-scale assay to shed light on the dynamics of cell motility. Combined with molecular dynamics models [48–50],

the proposed device for programmable subcellular adhesion/detachment will offer a platform for studies of molecular biomechanics of the cell, especially as related to mechanotransduction at the integrin-mediated focal adhesions [51,52].

References

- Geiger B, Bershadsky A, Pankov R, Yamada KM. Transmembrane crosstalk between the extracellular matrix and the cytoskeleton crosstalk. *Nat Rev Mol Cell Biol* 2001;2(11):793–805.
- Park TH, Shuler ML. Integration of cell culture and micro-fabrication technology. *Biotechnol Prog* 2003;19(2):243–53.
- Ridley AJ, Schwartz MA, Burridge K, Firtel RA, Ginsberg MH, Borisy G, et al. Cell migration: integrating signals from front to back. *Science* 2003;302(5651):1704–9.
- Beningo KA, Dembo M, Kaverina I, Small JV, Wang YL. Nascent focal adhesions are responsible for the generation of strong propulsive forces in migrating fibroblasts. *J Cell Biol* 2001;153(4):881–8.
- Zamir E, Geiger B. Molecular complexity and dynamics of cell-matrix adhesions. *J Cell Sci* 2001;114(20):3583–90.
- Galbraith CG, Yamada KM, Sheetz MP. The relationship between force and focal complex development. *J Cell Biol* 2002;159(4):695–705.
- Wiesner S, Legate KR, Fässler R. Integrin-actin interactions. *Cell Mol Life Sci* 2005;62(10):1081–99.
- Bershadsky A, Kozlov M, Geiger B. Adhesion-mediated mechanosensitivity: a time to experiment, and a time to theorize. *Curr Opin Cell Biol* 2006;18(5):472–81.
- Palecek SP, Loftus JC, Ginsberg MH, Lauffenburger DA, Horwitz AF. Integrin-ligand binding properties govern cell migration speed through cell-substratum adhesiveness. *Nature* 1997;385(6616):537–40.
- Clark P, Connolly P, Curtis AS, Dow JA, Wilkinson CD. Topographical control of cell behavior. *J Simple Step Cues Dev* 1987;99(3):439–48.
- Chehroudi B, Gould TR, Brunette DM. Titanium-coated micromachined grooves of different dimensions affect epithelial and connective-tissue cells differently *in vivo*. *J Biomed Mater Res A* 1990;24(9):1203–19.
- Lussi JW, Tang C, Kuenzi P-A, Staufner U, Csucs G, Vörös J, et al. Selective molecular assembly patterning at the nanoscale: a novel platform for producing protein patterns by electron-beam lithography on SiO₂/indium tin oxide-coated glass substrates. *Nanotechnology* 2005;16(9):1781–6.
- Lee K-B, Park SJ, Mirkin CA, Smith JC, Mrksich M. Protein nanoarrays generated by dip-pen nanolithography. *Science* 2002;295(5560):1702–5.
- Hoff JD, Cheng L-J, Meyhöfer E, Guo LJ, Hunt AJ. Nanoscale protein patterning by imprint lithography. *Nano Lett* 2004;4(5):853–7.
- Chen CS, Mrksich M, Huang S, Whitesides GM, Ingber DE. Geometric control of cell life and death. *Science* 1997;276(5317):1425–8.
- Lee NY, Lim JR, Kim YS. Selective patterning and immobilization of biomolecules within precisely-defined micro-reservoirs. *Biosens Bioelectron* 2006;21(11):2188–93.
- Folch A, Jo BH, Hurtado O, Beebe DJ, Toner M. Microfabricated elastomeric stencils for micropatterning cell cultures. *J Biomed Mater Res A* 2000;52(2):346–53.
- Roth EA, Xu T, Das M, Gregory C, Hickman JJ, Boland T. Inkjet printing for high-throughput cell patterning. *Biomaterials* 2004;25(17):3707–15.
- Birkbeck AL, Flynn RA, Ozkan M, Song D, Gross M, Esener SC. VCSEL arrays as micromanipulators in chip-based biosystems. *Biomed Microdevices* 2003;5(1):47–54.
- Ozkan M, Pisanic T, Scheel J, Barlow C, Esener S, Bhatia SN. Electro-optical platform for the manipulation of live cells. *Langmuir* 2003;19(5):1532–8.
- Rosenthal A, Voldman J. Dielectrophoretic traps for single-particle patterning. *Biophys J* 2005;88(3):2193–205.
- Lahann J, Mitragotri S, Tran T-N, Kaido H, Sundaram J, Choi IS, et al. A reversibly switching surface. *Science* 2003;299(5605):371–4.
- Truskey GA, Pirone JS. The effect of fluid shear stress upon cell adhesion to fibronectin-treated surfaces. *J Biomed Mater Res A* 1990;24(10):1333–53.
- van Kooten TG, Schakenraad JM, van der Mei HC, Dekker A, Kirkpatrick CJ, Busscher HJ. Fluid shear induced endothelial cell detachment from glass: influence of adhesion time and shear stress. *Med Eng Phys* 1994;16(6):506–12.
- García AJ, Huber F, Boettiger D. Force required to break $\alpha_5\beta_1$ integrin-fibronectin bonds in intact adherent cells is sensitive to integrin activation state. *J Biol Chem* 1998;273(18):10988–93.
- Cargill RSH, Dee KC, Malcolm S. An assessment of the strength of NG108-15 cell adhesion to chemically modified surfaces. *Biomaterials* 1999;20(23–24):2417–25.
- Kuo SC, Lauffenburger DA. Relationship between receptor/ligand binding affinity and adhesion strength. *Biophys J* 1993;65(5):2191–200.
- Kuo SC, Hammer DA, Lauffenburger DA. Simulation of detachment of specifically bound particles from surfaces by shear flow. *Biophys J* 1997;73(1):517–31.
- Goldstein AS, DiMilla PA. Effect of adsorbed fibronectin concentration on cell adhesion and deformation under shear on hydrophobic surfaces. *J Biomed Mater Res A* 2002;59(4):665–75.
- McClay DR, Wessel GM, Marchase RB. Intercellular recognition: quantitation of initial binding events. *Proc Natl Acad Sci U S A* 1981;78(8):4975–9.

- [31] Lotz MM, Burdsal CA, Erickson HP, McClay DR. Cell adhesion to fibronectin and tenascin: quantitative measurements of initial binding and subsequent strengthening response. *J Cell Biol* 1989;109(4):1795–805.
- [32] Burdsal CA, Alliegro MC, McClay DR. Tissue-specific, temporal changes in cell adhesion to echinonectin in the sea urchin embryo. *DevBiol* 1991;144(2):327–34.
- [33] Burdsal CA, Lotz MM, Miller J, McClay DR. A quantitative switch in integrin expression accompanies differentiation of F9 cells treated with retinoic acid. *DevDyn* 1994;201(4):344–53.
- [34] Sung KL, Sung LA, Crimmins M, Burakoff SJ, Chien S. Determination of junction avidity of cytolytic T cell and target cell. *Science* 1986;234(4782):1405–8.
- [35] Evans E, Ritchie K, Merkel R. Sensitive force technique to probe molecular adhesion and structural linkages at biological interfaces. *Biophys J* 1995;68(6):2580–7.
- [36] Shao J-Y, Hochmuth RM. Micropipette suction for measuring piconewton forces of adhesion and tether formation from neutrophil membranes. *Biophys J* 1996;71(5):2892–901.
- [37] Richards RG, ap Gwynn I, Bundy KJ, Rahn BA. Microjet impingement followed by scanning electron microscopy as a qualitative technique to compare cellular adhesion to various biomaterials. *Cell Biollnt*. 1995;19(12):1015–24.
- [38] Jiang X, Bruzewicz DA, Wong AP, Piel M, Whitesides GM. Directing cell migration with asymmetric micropatterns. *ProcNatlAcadSci U S A* 2005;102(4):975–8.
- [39] Inaba R, Khademhosseini A, Suzuki H, Fukuda J. Electrochemical desorption of self-assembled monolayers for engineering cellular tissues. *Biomaterials* 2009;30(21):3573–9.
- [40] Guillaume-Gentil O, Gabi M, Zenobi-Wong M, Vörös J. Electrochemically switchable platform for the micro-patterning and release of heterotypic cell sheets. *Biomed Microdevices* 2011;13(1):221–30.
- [41] Karp G. *Cell and molecular biology: concepts and experiments*. New York: John Wiley & Sons; 2005.
- [42] Dalton BA, Walboomers XF, Dziegielewski M, Evans MD, Taylor S, Jansen JA, et al. Modulation of epithelial tissue and cell migration by microgrooves. *J Biomed Mater Res A* 2001;56(2):195–207.
- [43] Yoon S-H, Lee C, Mofrad MRK. Viscoelastic characterization of the retracting cytoskeleton using subcellular detachment. *ApplPhysLett* 2011;98(13):133701.
- [44] Haga H, Sasaki S, Kawabata K, Ito E, Ushiki T, Sambongi T. Elasticity mapping of living fibroblasts by AFM and immunofluorescence observation of cytoskeleton. *Ultramicroscopy* 2000;82(1–4):253–8.
- [45] Haga H, Nagayama M, Kawabata K. Imaging mechanical properties of living cells by scanning probe microscopy. *CurrNanosci* 2007;3(1):97–103.
- [46] Mofrad MRK. Rheology of the cytoskeleton. *Annu Rev Fluid Mech* 2009;41:433–53.
- [47] Jamali Y, Azimi M, Mofrad MRK. A sub-cellular viscoelastic model for cell population mechanics. *PLoS One* 2010;5(8):e12097.
- [48] Lee SE, Chunsrivirod S, Kamm RD, Mofrad MRK. Molecular dynamics study of talin–vinculin binding. *Biophys J* 2008;95(4):2027–36.
- [49] Golji J, Mofrad MRK. A molecular dynamics investigation of vinculin activation. *Biophys J* 2010;99(4):1073–81.
- [50] Golji J, Lam J, Mofrad MRK. Vinculin activation is necessary for complete talin binding. *Biophys J* 2011;100(2):332–40.
- [51] Bao G, Kamm RD, Thomas W, Hwang W, Fletcher DA, Grodzinsky AJ, et al. Molecular biomechanics: the molecular basis of how forces regulate cellular function. *Mol Cell Biomech* 2010;3(2):91–105.
- [52] Mofrad MRK, Kamm RD. *Cellular mechanotransduction: diverse perspectives from molecules to tissues*. New York: Cambridge University Press; 2010.